## Hamiltonian chaos for one particle with two waves: Selfconsistent dynamics **⊘**

Matheus J. Lazarotto **□** ; Iberê L. Caldas **□** ; Yves Elskens **□** 



Chaos 35, 053143 (2025)

https://doi.org/10.1063/5.0261013





### Articles You May Be Interested In

Island myriads in periodic potentials

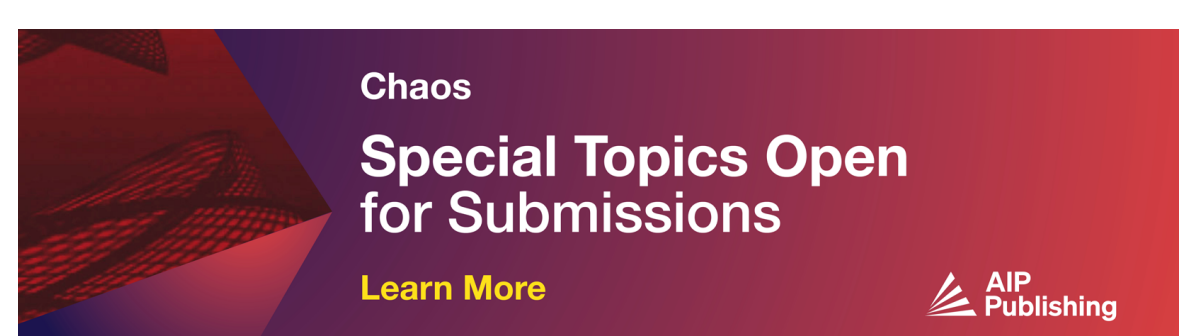
Chaos (March 2024)

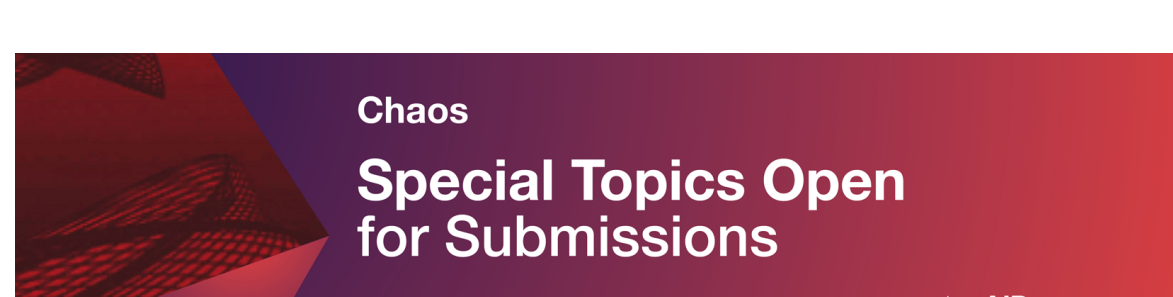
Low-dimensional chaos in the single wave model for self-consistent wave-particle Hamiltonian

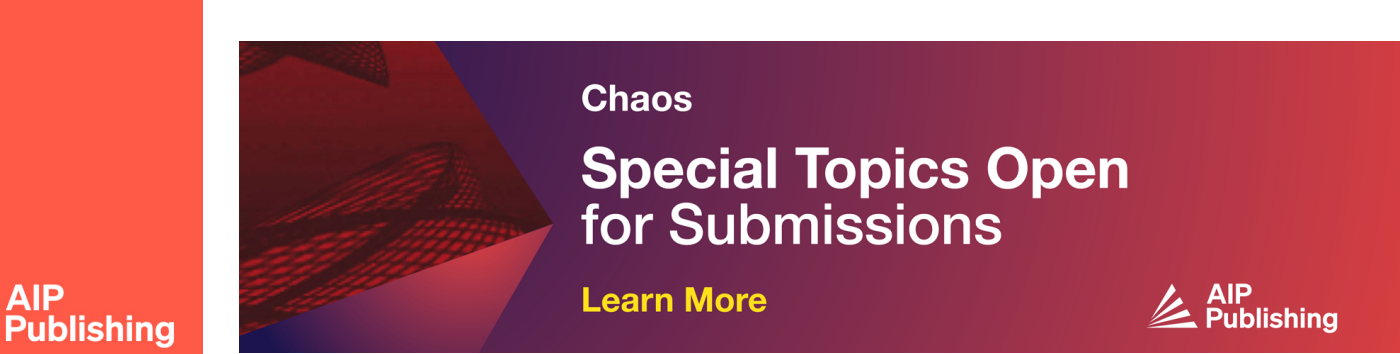
Chaos (August 2021)

Wave-particle interactions in a long traveling wave tube with upgraded helix

Phys. Plasmas (September 2020)









# Hamiltonian chaos for one particle with two waves: Self-consistent dynamics

Cite as: Chaos 35, 053143 (2025); doi: 10.1063/5.0261013 Submitted: 28 January 2025 · Accepted: 25 April 2025 · Published Online: 15 May 2025







Matheus J. Lazarotto, 1,2,a) D Iberê L. Caldas, 2,b) D and Yves Elskens 1,c)







#### **AFFILIATIONS**

Aix-Marseille Université, CNRS, UMR 7345, PIIM, F-13397, Marseille cedex 13, France

Note: This paper is part of the Special Topic on Complex Dynamical Systems, Nonlinear and Condensed Matter Physics: Dedicated to Serge Aubry.

a) Author to whom correspondence should be addressed: matheus\_jean\_l@hotmail.com

#### **ABSTRACT**

A simple model of wave-particle interaction is studied in its self-consistent form, that is, where the particles are allowed to feedback on the wave dynamics. We focus on the configurations of locked solutions (equilibria) and how the energy-momentum exchange mechanism induces chaos in the model. As we explore the system, we analyze the mathematical structure that gives rise to locked states and how the model's non-linearity enables multiple equilibrium amplitudes for waves. We also explain the predominance of regularity as we vary the control parameters and the mechanism behind the emergence of chaos under limited parameter choices.

Published under an exclusive license by AIP Publishing. https://doi.org/10.1063/5.0261013

When modeling physical systems composed of waves and particles, it is often assumed that the latter are subject to the influence of the former, but not the other way around. In this work, we investigate the effect of considering the mutual interaction between waves and particles, resulting in a self-consistent dynamics. With a Hamiltonian model of the system, we consider the case of one particle interacting with two waves. We first reduce the equations from a six-dimensional problem to a four-dimensional one, with one constant of the motion, enabling better handling of equations and visualization of their solutions. While previous studies analyzed how a particle influenced by two free waves—i.e., without mutual interaction—behaves chaotically, here we discuss how the particle serves as a mediator, enabling the exchange of energy and momentum between the waves and propagating its chaotic motion into their evolution. Moreover, we find that several locked states, where both waves travel in equilibrium with the particle, can exist for the same total momentum and energy.

#### I. INTRODUCTION

When describing a plasma on a microscopic scale, a fundamental process is the interaction between its particles

(electrons and ions) and waves propagating in the plasma.<sup>1,2</sup> In the particular limit of collisionless plasmas, that is, when the time scale of particle "collisions" is much longer than the time scale of the interaction with waves, the energy and momentum exchange between particles and waves becomes relevant to the point of generating instabilities, favoring wave amplification or particle

For instance, this scenario can be experimentally reproduced in traveling wave tubes (TWTs), where a beam of electrons interacts with electrostatic waves in a controllable environment.<sup>4,5</sup> This setup enables the analysis of chaotic interactions due to the energymomentum exchange that may lead to instabilities and further turbulence in plasmas, which, in turn, correlates to the emergence of chaotic regions in phase space. This chaotic transition can be caused by resonance overlap of the waves, nonlinear synchronization by a single nonresonant wave or the "devil's staircase" mechanism, causing a spread of the velocity distribution of the beam.<sup>6,7</sup> Stability islands, on the other hand, can correlate with coherent particle acceleration (beam trapping), and the breaking of barriers (invariant tori in the one-particle phase space), allowing for new ways of chaos control.

When modeling such scenarios, the Langmuir waves, that is, the collective vibration of electrons in the presence of much heavier

<sup>&</sup>lt;sup>2</sup>Instituto de Física, Universidade de São Paulo, Rua do Matão 1371, São Paulo 05508-090, Brazil

b) ibere@if.usp.br

c)yves.elskens@univ-amu.fr

ions that neutralize the system, are found to be coupled with quasi-resonant particles (i.e., an electron's velocity being close to a wave's phase velocity). Thus, for simplicity, the usual Hamiltonian models initially consider only the effect of waves on the particles. To give a step ahead, the re-interaction of the particles with the waves can be taken into account, thereby making the dynamics self-consistent.  $^{1,2,9}$  Consequently, electrons (and ions) do not play just the role of test particles but, instead, promote energy-momentum exchange with the waves, allowing for the aforementioned nonlinear phenomena. To model it, one can consider M independent Langmuir waves behaving as harmonic oscillators and N quasi-resonant free charged particles, with the addition of a coupling term for each wave-particle pair.  $^{10-12}$ 

Gomes *et al.*<sup>13</sup> considered two of the simplest cases, namely, that of one wave and one particle (M=1,N=1), which is analytically treatable and shows the electron either being trapped (strong resonance) or passing through wave potential wells, <sup>14,15</sup> and the case of one wave interacting with two particles (M=1,N=2), that presents chaotic behavior. We direct the reader to the work of Gomes *et al.*<sup>13</sup> for a simple yet broad introduction on the experimental context, modeling, and applications of wave-particle dynamics.

In this sense, our work is complementary to Gomes' work, for we consider the remaining case of two waves interacting with one particle (M=2,N=1), aiming to a simple description of the interaction between waves and particles. By studying these simplest cases, one may shed light on the microscopic mechanisms that induce chaos in the macroscopic system and how to prevent (or allow) it. In the current work, for instance, it is shown that equilibrium solutions only come in locked configurations and allow multiple unstable wave amplitude combinations. The emergence of chaos in the system is predominantly due to separatrix chaos related to the parameter limit where non-linear coupling produces energy-momentum exchange.

In what follows, Sec. II A starts by presenting the generic wave-particle self-consistent Hamiltonian model and, Sec. II B, the particular case studied here (for M=2,N=1), along with its mathematical simplification to reduce the number of degrees of freedom and number of parameters. Section III presents a global analysis of the equilibrium solutions in parameter space. Section IV discusses the emergence of chaos in phase space and the integrable limits of the system. Appendix sections provide more details on model parameter simplifications, the stability of equilibrium solutions, and the decoupling limit of the system equations of motion.

#### II. THE WAVE-PARTICLE HAMILTONIAN

#### A. The generic model

Within the context of Langmuir waves interacting with ions in plasmas, one can model the self-consistent dynamics of N identical particles traveling in a periodically bounded interval of length L via a coupling with M longitudinal waves. Each particle is described by the generalized coordinate-momentum pairs  $(x_i, p_i)$  and each wave is written in phasor formulation as  $Z_j = X_j + \mathrm{i} Y_j = \sqrt{2I_j} \, \mathrm{e}^{-\mathrm{i}\theta_j}$ , with either Cartesian  $(X_j, Y_j)$  or polar  $(\theta_j, I_j)$  canonical variables. Within this interval, wave numbers are given by  $k_j = \frac{2\pi j}{L}$ , for  $j \in \mathbb{Z}$ , and

natural frequencies by  $\omega_{0i}$ . The system's Hamiltonian is then<sup>1,2</sup>

$$H_{sc}^{N,M} = \sum_{i=1}^{N} \frac{p_i^2}{2m} + \sum_{j=1}^{M} \omega_{0j} \frac{X_j^2 + Y_j^2}{2} + \epsilon \sum_{i=1}^{N} \sum_{i=1}^{M} \frac{\beta_j}{k_j} \left( Y_j \sin(k_j x_i) - X_j \cos(k_j x_i) \right), \tag{1}$$

or, equivalently, in polar-phasor coordinates,

$$H_{\text{sc}}^{N,M} = \sum_{i=1}^{N} \frac{p_i^2}{2m} + \sum_{j=1}^{M} \omega_{0j} I_j - \epsilon \sum_{i=1}^{N} \sum_{j=1}^{M} \frac{\beta_j}{k_j} \sqrt{2I_j} \cos(k_j x_i - \theta_j),$$

with  $\beta_j$  as a coupling constant with the *j*th-wave and  $\epsilon$  an overall coupling scale. For the wave degrees of freedom,  $X_j$  and  $\theta_j$  are treated as coordinates with  $Y_i$  and  $I_i$  as their respective conjugate momenta.

as coordinates with  $Y_j$  and  $I_j$  as their respective conjugate momenta. Hamiltonian  $H_{sc}^{N,M}$  comprises three contributions: the free motion (kinetic energy) of particles (m>0); the harmonic oscillation of waves  $(\omega_{0j}>0)$ ; and the coupling between particles and waves. Furthermore, Hamiltonian  $H_{sc}^{N,M}$  is invariant under translations in time and in space, so that the total energy  $E=H_{sc}^{N,M}$  and the total momentum  $P=\sum_{i=1}^N p_i + \sum_{j=1}^M k_j I_j$  are conserved. The latter constant reveals that the growth or decay of a wave with positive phase velocity  $(\frac{\omega_{0j}}{k_j}>0)$  is directly balanced with the slowing down or acceleration of particles. On interchanging the time and space variables, this Hamiltonian also captures the key physics in the dynamics of traveling wave tubes.<sup>2,4</sup> For instance, in the paradigmatic two-wave scenario with a slaved particle, given parameters  $\epsilon \beta_1 = \epsilon \beta_2 = \beta$ ,  $k_1 = k_2 = k$ , m, the Chirikov overlap parameter is  $s = 2\sqrt{\beta k/m}((2I_1)^{1/4} + (2I_2)^{1/4})/|\omega_1 - \omega_2|$ .

#### B. The single particle with two waves

To address the key physics of the system, one can start looking at the simpler scenarios, namely, those with few waves and particles interacting with each other. The simplest case, that of M=N=1, is integrable and was treated before in Refs. 13–15; thanks to its integrability, it provides reference information for the more complex cases where chaos emerges. With the addition of a particle (N=2, M=1), as studied by Gomes  $et\ al.$ , 13 the non-linear term in Hamiltonian (1) implies the emergence of chaos in phase space not only around separatrices but also near elliptic points.

Here, we consider the "mirror" case of one particle coupled to two waves, that is, the case with N=1, M=2 in Hamiltonian (1) and (2). The system, thus, has seven free parameters:  $k_1, k_2, \epsilon \beta_1, \epsilon \beta_2, \omega_{01}, \omega_{02}$ , and m (along with three free scales, leaving four dimensionless free parameters). For simplicity,  $\epsilon \beta_j$  are selected to be equal and unity:  $\epsilon \beta_1 = \epsilon \beta_2 = 1$ , as well as the particle mass: m=1, which can be set without the loss of generality by rescaling variables (see Appendix A for more details).

Given the translational invariance, only the relative positions  $\theta_j - k_j x$  are dynamically relevant; thus, for commensurate  $k_1$  and  $k_2$ , the particle position x can meet periodic boundary conditions,  $x \in [0, L]$ , compatible with both waves. For incommensurate wave numbers, the position space is necessarily the full real line. By setting

equal wave numbers and given a proper rescaling of space, we select  $k_1 = k_2 = 1$  (in order to keep free phase-velocities, the frequencies  $\omega_{0i}$  are kept different).

The resulting three degrees-of-freedom Hamiltonian is autonomous and translation-invariant; in Cartesian-phasor coordinates, it reads

$$H_{sc}^{1,2} = \frac{p^2}{2} + \omega_{01} \frac{X_1^2 + Y_1^2}{2} + \omega_{02} \frac{X_2^2 + Y_2^2}{2} + (Y_1 + Y_2) \sin(x) - (X_1 + X_2) \cos(x), \tag{3}$$

and, likewise, in polar-phasor form,

$$H_{\rm sc}^{1,2} = \frac{p^2}{2} + \omega_{01}I_1 + \omega_{02}I_2 - \sqrt{2I_1}\cos(x - \theta_1) - \sqrt{2I_2}\cos(x - \theta_2). \tag{4}$$

To further simplify the model and better visualize the solutions in phase space, it is convenient to reduce the number of degrees of freedom, which is obtained with a simple sequence of canonical transformations. Although assuming equal wavelengths and coupling strengths, the transformations below do not depend on these assumptions.

The particle's degree of freedom can be suppressed with the aid of the total momentum constant P using  $p = P - I_1 - I_2$ . In addition, a Galilean transformation to a reference frame traveling with the first wave, provided by the generating function

$$\begin{split} G(x,\theta_1,\theta_2,\bar{p},\bar{I}_1,\bar{I}_2) &= (x-\omega_{01}t)(\bar{p}+\omega_{01}) + (\theta_1-\omega_{01}t)\bar{I}_1 \\ &+ (\theta_2-\omega_{01}t)\bar{I}_2 + \frac{\omega_{01}^2t}{2}, \end{split}$$

and the definition of the relative angle  $\phi_j:=\bar{\theta}_j-\bar{x}=\theta_j-x$ , provided by the generating function

$$F(\bar{x}, \bar{\theta}_1, \bar{\theta}_2, p', I'_1, I'_2) = I'_1(\bar{\theta}_1 - \bar{x}) + I'_2(\bar{\theta}_2 - \bar{x}) + p'\bar{x},$$

simplify Hamiltonian (4) to

$$H' = \frac{\left(I_1' + I_2'\right)^2}{2} - \bar{P}\left(I_1' + I_2'\right) + \Delta_{\omega}I_2' - \sqrt{2I_1'}\cos(\phi_1) - \sqrt{2I_2'}\cos(\phi_2), \tag{5}$$

where prime symbols denote the final transformed variables  $(x, \theta_j, p, I_j) \stackrel{G}{\mapsto} (\bar{x}, \bar{\theta}_j, \bar{p}, \bar{I}_j) \stackrel{F}{\mapsto} (x', \phi_j, p', I'_j)$  and will be dropped from now on.

From old to new variables, the amplitudes are unmodified  $(I_j'=I_j)$  and the new angles are the relative position between the particle and the wave  $\phi_j=\theta_j-x$ . The new total momentum is now  $\bar{P}=P-\omega_{01}$  and we define the detuning parameter between the waves:  $\Delta_\omega:=\omega_2-\omega_1$ , eliminating one of the frequencies. This final form has two degrees of freedom  $(\phi_1,\phi_2)$ , their associated momenta  $(I_1,I_2)$ , and three control parameters  $(H,\bar{P},\Delta_\omega)$ ; Hamiltonian H itself being a constant of the motion. The frequency  $\omega_{01}$  can be set to zero without loss of generality.

In Cartesian variables, Hamiltonian (3) in simplified form reads

$$H' = \frac{1}{8} \left( u_1^2 + v_1^2 + u_2^2 + v_2^2 \right)^2 - \frac{\bar{P}}{2} \left( u_1^2 + v_1^2 + u_2^2 + v_2^2 \right) + \frac{\Delta_{\omega}}{2} \left( u_2^2 + v_2^2 \right) - u_1 - u_2, \tag{6}$$

where

$$u_i = \sqrt{2I_i}\cos(\phi_i), \quad v_i = \sqrt{2I_i}\sin(\phi_i),$$
 (7)

for i = 1, 2.

It may be of interest to keep both forms since Cartesian coordinates provide a smooth transition for the limit  $I_j \rightarrow 0$ , though the polar ones provide a more intuitive picture of the dynamics. Appendix B shows the equations of motion in Cartesian form.

It is worth mentioning that Hamiltonian (6) is fourth degree in both  $u_i$  and  $v_i$ , making the visualization of phase space via Poincaré sections less straightforward. Since the intersection of trajectories with the section may yield two positive (or negative) roots, the usual method of fixing a position (say  $u_2 = 0$ ) and a sign condition on the conjugate momentum (say  $v_2 > 0$ ), is not enough to produce a uniquely defined map. Since extra roots may exist and appear over the points of map made by the first set of roots, invariant circles appear overlapping. A solution can be achieved by filtering these two sets of roots with an extra condition as  $\dot{u}_2 > 0$ .

#### III. LOCKED SOLUTIONS

As a reference for the system's global dynamics, one can look at the equilibrium solutions [i.e.,  $(\dot{I}_1, \dot{I}_2, \dot{\phi}_1, \dot{\phi}_2) = \vec{0}$ ] of the equations of motion provided by Hamiltonian (5),

$$\dot{I}_{1} = -\partial_{\phi_{1}}H' = -\sqrt{2I_{1}}\sin(\phi_{1}), 
\dot{I}_{2} = -\partial_{\phi_{2}}H' = -\sqrt{2I_{2}}\sin(\phi_{2}), 
\dot{\phi}_{1} = \partial_{I_{1}}H' = (I_{1} + I_{2}) - \bar{P} - \frac{\cos(\phi_{1})}{\sqrt{2I_{1}}}, 
\dot{\phi}_{2} = \partial_{I_{2}}H' = (I_{1} + I_{2}) - \bar{P} + \Delta_{\omega} - \frac{\cos(\phi_{2})}{\sqrt{2I_{2}}}.$$
(8)

In the present context, equilibrium solutions are also referred to as locked states, given that, when in equilibrium, the amplitude equations  $(\dot{I}_1,\dot{I}_2)$  yield the condition that the relative phases are constant  $(\phi_i^* \in \{0,\pi\}, \text{ for } i=1,2)$  meaning that both waves and the particle travel at the same velocity with the latter constrained to be at either the minimum or maximum of one of the waves while the other is in phase or anti-phase. It is worth mentioning that the last two equations in (8) prevent the existence of zero-wave solutions  $[I_1(t)=I_2(t)=0]$  for both waves simultaneously for generic  $(\bar{P},\Delta_\omega)$ . For single null waves, i.e.,  $I_1^*=0\neq I_2^*$  (or vice versa), it is possible to obtain such solutions for  $\Delta_\omega=0$ . In such a case, the null wave has an indefinite phase  $\phi_i$  and the remaining one must have a fixed amplitude given by the total momentum  $\bar{P}$ . Other considerations on the  $\Delta_\omega=0$  case are discussed in Appendix C.

From the locked relative phases  $\phi_1^* = n_1 \pi$  and  $\phi_2^* = n_2 \pi$ , for  $n_i = 0, 1$  and i = 1, 2, the equilibrium amplitudes  $I_1^*$  and  $I_2^*$ , thus,

**FIG. 1.** Color map with the number of equilibrium solutions for different  $n_2$ . (Left) case  $\phi_2^*=0$ ; (Right) case  $\phi_2^*=\pi$ .

must satisfy

$$\frac{\cos(n_2\pi)}{\sqrt{2I_2^*}} - \frac{\cos(n_1\pi)}{\sqrt{2I_1^*}} = \Delta_{\omega}.$$
 (9)

Therewith, the relation between amplitudes enables one to find  $(I_1^*, I_2^*)$  by substituting Eq. (9) into  $\dot{I_1} = 0$ , yielding

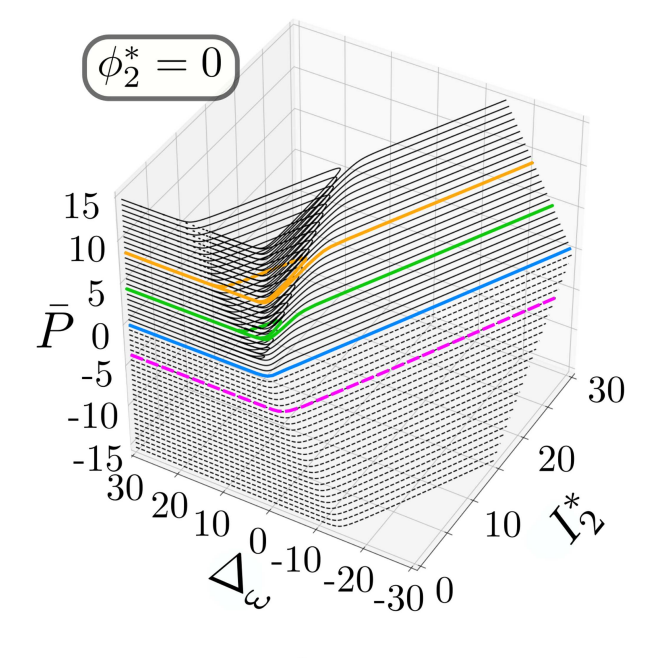
$$R(I_{2}, n_{2}) = I_{2}\sqrt{2I_{2}} \left( 1 + \left( (-1)^{n_{2}} - \Delta_{\omega}\sqrt{2I_{2}} \right)^{2} \right) + \left( \left( \Delta_{\omega} - \bar{P} \right) \sqrt{2I_{2}} - (-1)^{n_{2}} \right) \left( (-1)^{n_{2}} - \Delta_{\omega}\sqrt{2I_{2}} \right)^{2}.$$
(10)

Solutions are then given by the condition  $R(I_2^*, n_2) = 0$ , with each one amounting for two locked states  $(I_1^*, I_2^*, n_1\pi, n_2\pi)$ , namely, one with  $n_1 = 0$  and the other with  $n_1 = 1$ . The existence of roots to condition (10) was evaluated numerically by scanning over the parameter space  $(\bar{P}, \Delta_\omega)$ , with the result shown in Fig. 1 for both cases  $n_2 = 0$  and  $n_2 = 1$ .

In order to clarify the dependence of the number of roots as the control parameters change, Fig. 2 shows the surface  $R(I_2^*)=0$  along with the  $I_2^*$  axis. In this plot, roots will exist whenever the  $I_2^*$  axis crosses the surface for fixed control parameters  $\bar{P}$  and  $\Delta_{\omega}$ .

For either case of  $\phi_2^*$ , the set of solutions is composed of two non-intersecting surfaces. One of them has a cup-like form, which asymptotically converges to  $I_2^* \to 0$  as  $\Delta_\omega \to \infty(-\infty)$  for  $\phi_2^* = 0$  ( $\phi_2^* = \pi$ ). The second surface branch, completely detached from the cup, presents different concavity in each scenario of  $\phi_2^*$ . When  $\phi_2^* = 0$ , the branch is convex and, therefore, allows for one crossing throughout all parameter space, whereas for  $\phi_2^* = \pi$ , the concave surface allows only for crossings up to the limit  $\Delta_\omega \lesssim 0$ . The appearance of two extra roots, in both cases, is due to the cup-like branch, since any intersection with it implies two extra solutions, although these are only possible for  $\bar{P} \gtrsim 1$ . It is worth pointing out that the reasoning above does not consider any constraint on the Hamiltonian H value.

From both Figs. 1 and 2, the case  $\phi_2^* = 0$  guarantees that it is always possible that the particle is placed at the minimum of one of the waves and that it is locked to travel at the same speed, regardless



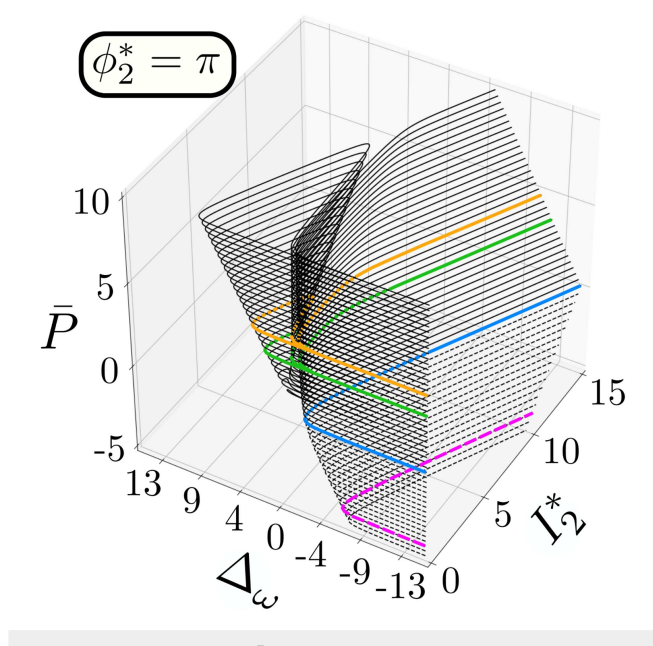


**FIG. 2.** Surface plot of  $R(I_2^*, \bar{P}, \Delta_\omega) = 0$  with its contour lines at different constant values of  $\bar{P}$ . Dashed (respectively, plain) lines correspond to  $\bar{P} < 0$  (respectively,  $\bar{P} > 0$ ). (Top)  $\phi_2^* = 0$  (viz.,  $n_2 = 0$ ); (Bottom)  $\phi_2^* = \pi$  (viz.,  $n_2 = 1$ ). Colored lines indicate particular values of  $\bar{P}$  for the stability analysis shown in Figs. 3–5.

of  $\bar{P}, \Delta_{\omega}$ . Moreover, if the total momentum of the system is large enough ( $\bar{P} \gtrsim 1$ ), new locked states become possible in which the waves may have enhanced or suppressed amplitude to provide the balance of forces acting on the particle.

30 May 2025 15:53:49

In addition to the solutions themselves, stability is promptly obtained from the system's Jacobian, which yields a simple biquadratic form (see Appendix D). Figures 3–5 show bifurcation diagrams over the contour lines shown in Fig. 2; in them, stable points (eigenvalues  $\lambda = ib$ , for  $b \in \mathbb{R}_{\neq 0}$ ) are colored blue, purely unstable points ( $\lambda \in \mathbb{R}_{\neq 0}$ ) are colored red, and complex unstable ( $\lambda = a + ib$  for  $a, b \in \mathbb{R}_{\neq 0}$ ) are colored green.

When analyzing stability, we now consider the combinations of locked phases including  $n_1$ , thus resulting in four possible scenarios of  $(n_1, n_2)$ . For  $(n_1, n_2) = (0, 0)$ , all solutions are stable.

For  $(n_1, n_2) = (0, 1)$ , Fig. 3 shows that the concave surface has its lower (upper) branch always stable (unstable). This indicates that at the expense of suppressing the second wave momentum, it is possible for wave 1 to carry the particle at its minimum. Similarly, as the total momentum increases and the cup bifurcation takes place, the upper (lower) half of the branch is unstable (stable). For  $\bar{P} > 0$ , the presence of complex unstable points amidst stable ones, in both branches, prevents the second wave amplitude growth while the particle is locked to wave 1.

For  $(n_1, n_2) = (1, 0)$ , Fig. 4 shows that higher values of  $I_2^*$  are now stable, indicating the opposite behavior to the one found previously for  $(n_1, n_2) = (0, 1)$ . Now, with the increase of the second wave amplitude, the stability of its minimum allows for the particle to be placed at the maximum of the first wave at the same time. Again, as the total momentum increases, stable branches become complexly unstable, but now preventing the locking for small  $I_2^*$  amplitudes, with small stability windows, particularly for  $\bar{P} = 0$  and  $\bar{P} = 8$ . Also, the cup-like surface provides a stable branch for detuning  $\Delta_{\omega}$  higher enough.

For  $(n_1, n_2) = (1, 1)$ , with the particle placed at the maxima of both waves simultaneously, the expected instability is found for most of the parameter space. However, Fig. 5 shows that for the total momentum that is negative enough, e.g.,  $\bar{P} = -4$ , or high enough, e.g.,  $\bar{P} = 4$ , branches with low  $I_2^*$  are stable, with no complex instability found. This indicates that at the expense of the second wave attenuation, the particle can be kept at an unexpected unstable position.

#### IV. POINCARÉ SECTIONS AND CHAOS

Once the three degrees-of-freedom Hamiltonian (3) [or in polar form (4)] is reduced to the equivalent 2-degree-of-freedom form (6) [or in polar form (5)], trajectories can be visualized in phase space. To this end, we made use of the Poincaré section defined as

$$\Sigma = \{ (\phi_1, \phi_2, I_1, I_2) \in \mathbb{R}^4; \ \phi_1 = \phi_2; \ \dot{\phi}_2 > 0 \}.$$
 (11)

From the selected Poincaré section, we measured the area of phase space occupied either by stability islands or chaotic regions as a function of the control parameters  $(\bar{P}, \Delta_{\omega}, H)$ , once fluctuations are expected, given the nonlinear nature of the model. For this purpose, the chaotic/regular areas were measured over the section  $\Sigma$  [Eq. (11)] via a smaller alignment index (SALI) method. We refrain from detailing the method here and direct the reader to the original reference as presented by Skokos. <sup>18,19</sup> Briefly, the algorithm integrates a single trajectory to numerically determine whether it is stable or chaotic, along with two deviation vectors evolved in tangent space according to the linearized equations of motion. Based on

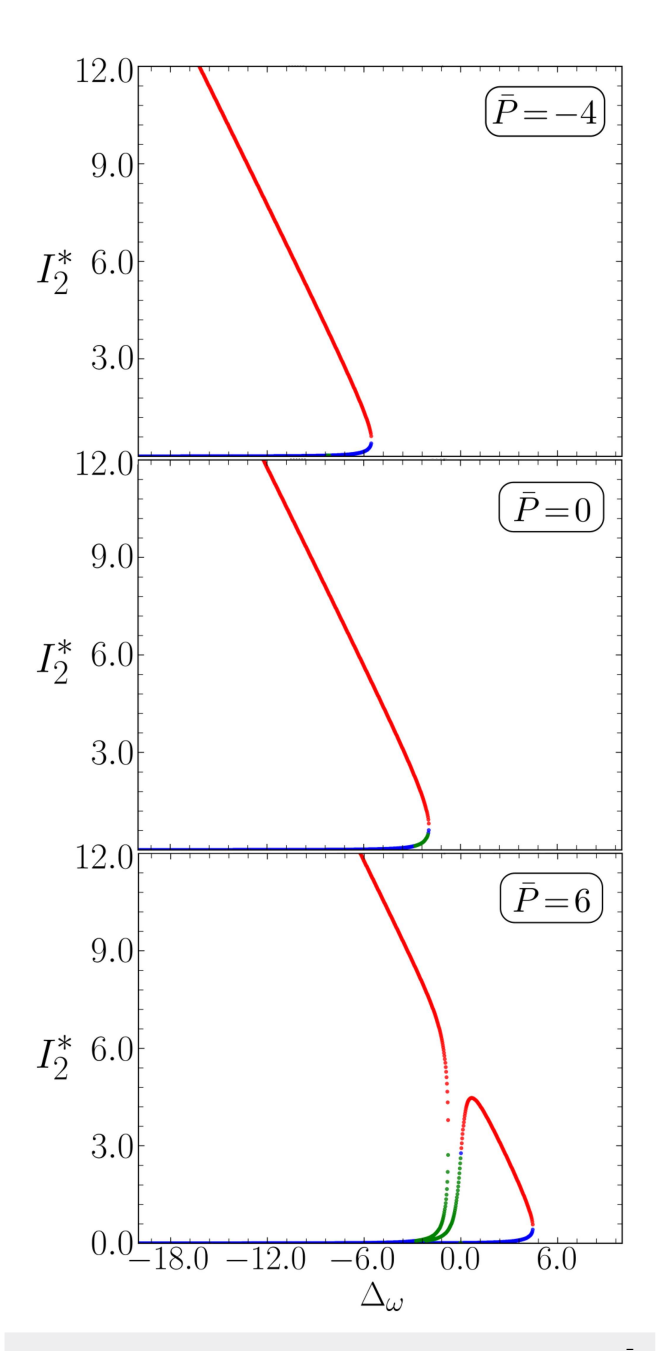


**FIG. 3.** Bifurcation diagram for  $n_1=0$ ,  $n_2=1$  for different values of fixed  $\bar{P}$ , corresponding to different horizontal lines from the bottom frame in Fig. 2. Colors indicate stability, with purely unstable points in red, stable points in blue, and complex unstable in green.  $\bar{P}=-4$ ,  $\bar{P}=0$ , and  $\bar{P}=6$  correspond, respectively, to the magenta, blue, and yellow curves in the bottom frame  $(\phi_2^*=\pi)$  of Fig. 2.

the local linearized geometry of phase space around the trajectory, the two deviation vectors align with each other along the unstable manifold direction, in case the trajectory is chaotic. On the other hand, when it is stable, the local geometry is a plane tangent to a

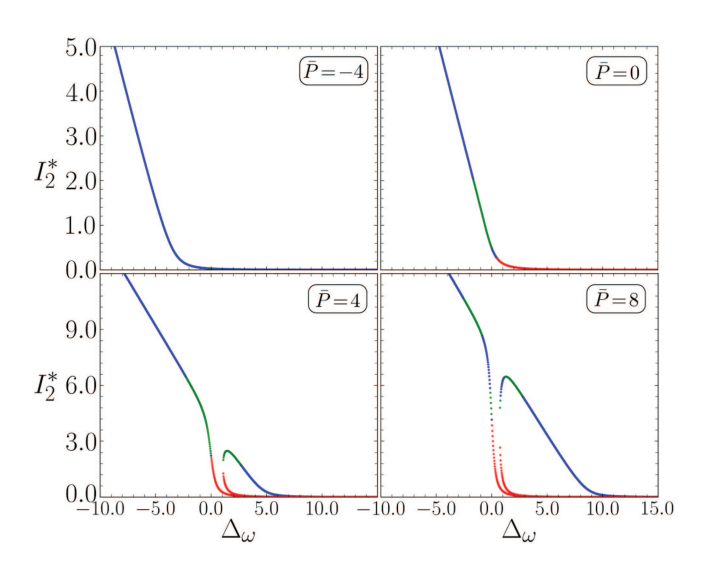


**FIG. 4.** Bifurcation diagram for  $n_1=1, n_2=0$  for different values of fixed  $\bar{P}$ , corresponding to different horizontal lines from the top frame in Fig. 2. Colors indicate stability, with purely unstable points in red, stable points in blue, and complex unstable in green.  $\bar{P}=-4, \bar{P}=0, \bar{P}=4,$  and  $\bar{P}=8$  correspond, respectively, to the magenta, blue, green, and yellow curves in the top frame  $(\phi_2^*=0)$  of Fig. 2.

torus to which the vectors become parallel while keeping their relative angle non-null. Therefore, the orbit is deemed chaotic if the deviation vectors align, or stable, in case they do not.

Running the SALI algorithm for each trajectory on a grid of initial conditions over the Poincaré section  $\Sigma$  for a given set  $(\bar{P}, \Delta_{\omega}, H)$  enables one to evaluate the percentage of stable area in phase space. By repeating this while scanning the parameters  $(\bar{P}, \Delta_{\omega})$ , we obtain the color maps seen in Fig. 6, where each panel corresponds to a different energy H value. It is worth noting that Hamiltonian (6) defines compact energy surfaces in the four-dimensional phase space, thus ensuring that the fractional area A is well defined.

The numerical integration of trajectories was made with an eighth-order Runge–Kutta–Dormand–Prince method with an adaptive step, for relative and absolute precisions  $\epsilon_{\rm abs} = \epsilon_{\rm rel} = 10^{-13}$ . In these conditions, the total energy (5) (E(t) = H) presented maximum deviations of  $|\delta E| = |E(t) - E_0| = 10^{-8}$ , with deviations at least one or two orders of magnitude smaller for smoother orbits. To avoid evaluations of inverse-square roots in Eq. (8), integration was carried using Hamiltonian (6) [Eq. (B1) in Appendix B] and converted to phasor coordinates when needed using (7).

For the SALI implementation, the initial deviation vectors  $\hat{\omega}_i = (\delta u_1, \delta u_2, \delta v_1, \delta v_2)$ , for i = 1, 2, were chosen orthogonal to each other for all initial conditions, with

$$\hat{\omega}_1 = (0, 1, 0, 0)$$
 and  $\hat{\omega}_2 = (0, 0, 0, 1)$ . (12)

The deviation vectors were normalized every  $\delta t=0.5$  time units to prevent overflow. The numerical threshold differentiating chaotic from regular orbits was SALI(t) <  $10^{-10}$ .

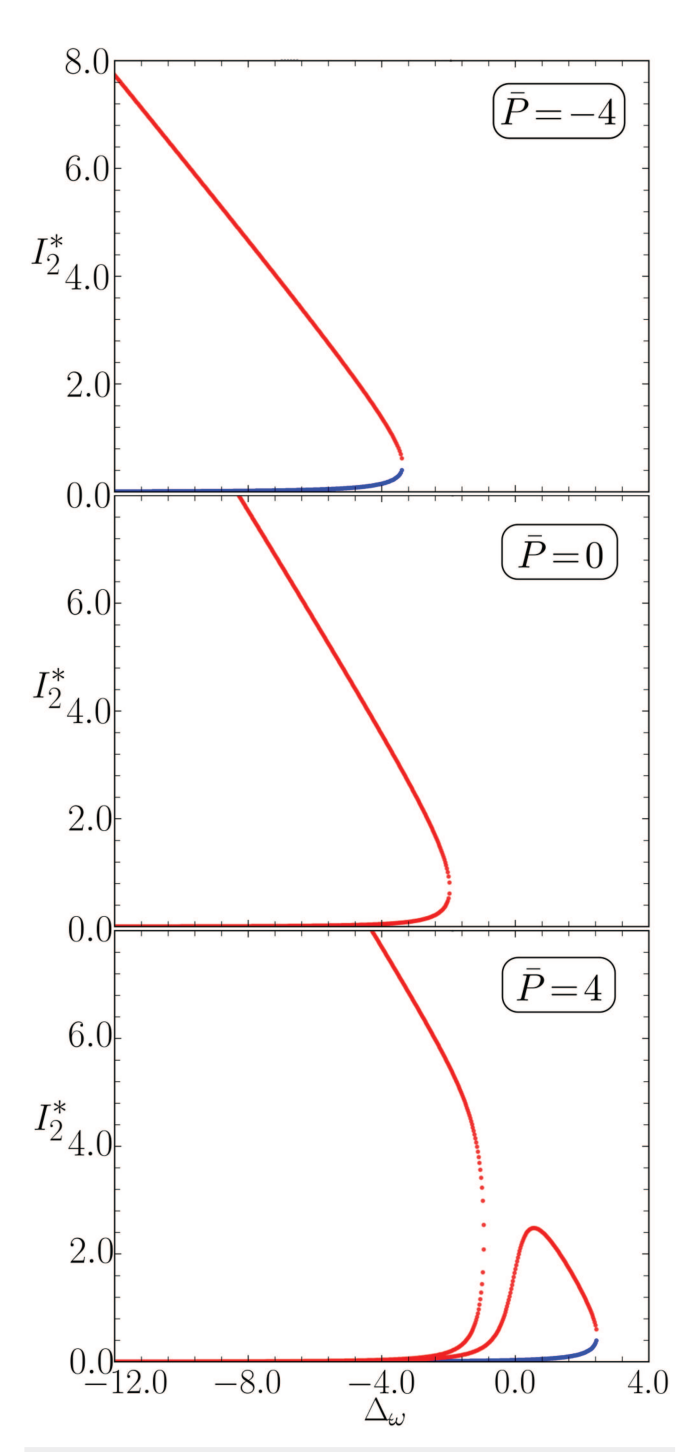


**FIG. 5.** Bifurcation diagram for  $n_1=1$ ,  $n_2=1$  for different values of fixed  $\bar{P}$ , corresponding to different horizontal lines from the bottom frame in Fig. 2. Colors indicate stability, with purely unstable points in red, stable points in blue, and complexly unstable in green.  $\bar{P}=-4$ ,  $\bar{P}=0$ , and  $\bar{P}=4$  correspond, respectively, to the magenta, blue, and green curves in the bottom frame  $(\phi_2^*=\pi)$  of Fig. 2.

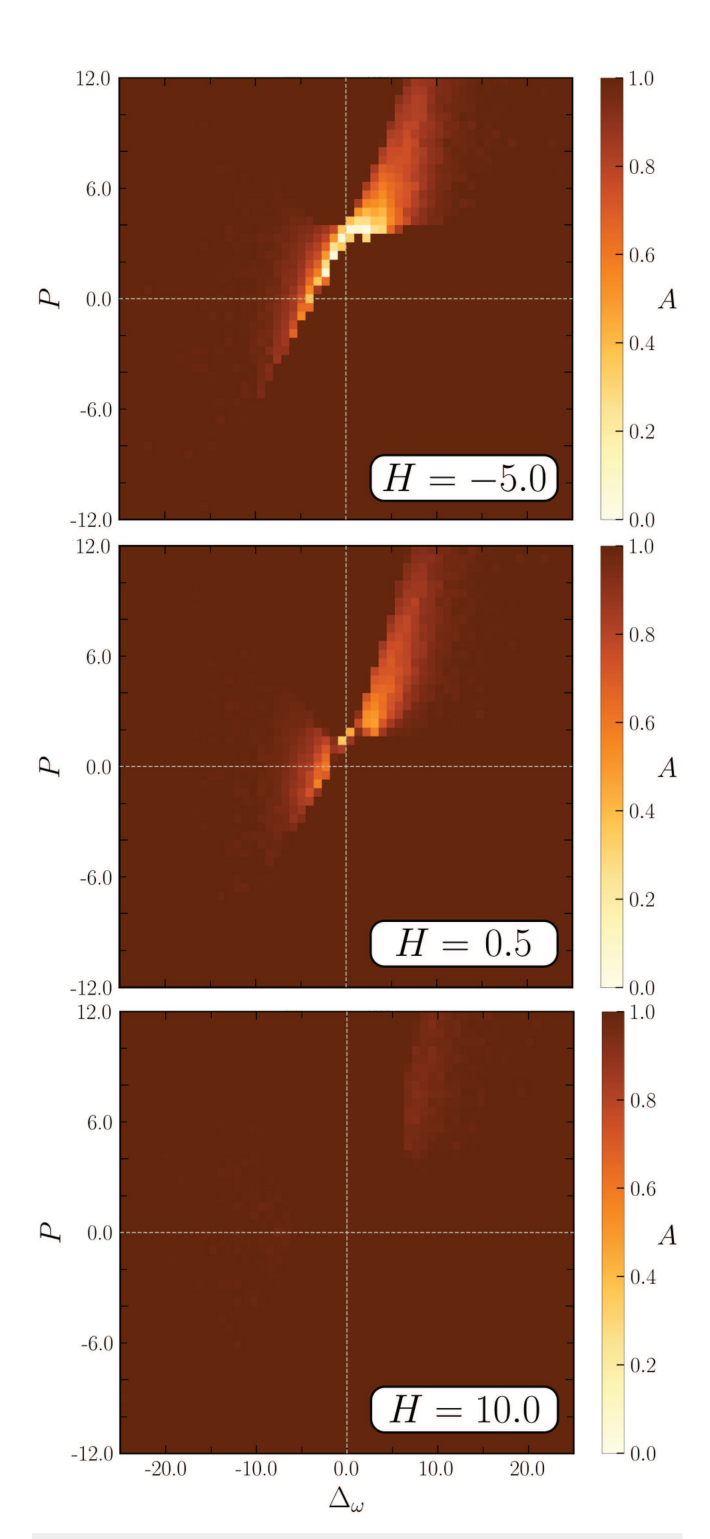


**FIG. 6.** Color map of the stable area portion in parameter space for multiple energies H. In the color bar, total chaos is given by A=0 and total regularity by A=1. Grid size is  $75\times75$ .

At first, the predominance of stability in the system becomes clear as, for most of the parameter space, the chaotic area is nearly zero (dark brown regions— $A\approx 1$ ). This should hold beyond the parameter space limits chosen here  $(\bar{P},\Delta_{\omega})\in[-12,12]\times[-25,25]$  as for either large  $|\bar{P}|$  or  $|\Delta_{\omega}|$ , the equations of motion become

$$\begin{split} \dot{I}_1 &\approx -\sqrt{2I_1}\sin(\phi_1), \\ \dot{I}_2 &\approx -\sqrt{2I_2}\sin(\phi_2), \\ \dot{\phi}_1 &\approx \pm |\bar{P}| - \frac{\cos(\phi_1)}{\sqrt{2I_1}}, \\ \dot{\phi}_2 &\approx \pm |\bar{P}| \pm |\Delta_{\omega}| - \frac{\cos(\phi_2)}{\sqrt{2I_2}}; \end{split} \tag{13}$$

noting that  $I_1$  and  $I_2$  are limited by the total energy E=H in Eq. (5). If either  $I_1$  or  $I_2$  is small (in view of the denominator for  $\dot{\phi}_i$ ), their amplitude have a limited growth rate once  $\phi_i$  evolves rapidly and the average increment in  $\dot{I}_1$  is zero or small, therefore generating a stable scenario. In case only  $|\Delta_{\omega}|$  is large,  $\phi_2$  and  $I_2$  become regular as well, resulting in a regular evolution for  $\phi_1$ . Therefore, for high enough values of  $|\bar{P}|$  and  $|\Delta_{\omega}|$ , stability should still dominate phase space, as the dynamics of waves uncouples and the system reduces to the paradigmatic M=N=1 case, which is analytically treatable.  $^{13-15}$  More details on the dynamics for weak coupling are given in Appendix E.

Despite this predominance of stability, a prominent chaotic region appears at lower values of total momentum and frequency detuning, which decreases for large energy and eventually vanishes for  $H \approx 10$  (Fig. 6). Similar to what was previously discussed, the suppression of chaos for increasing energy is due to the dominance of the wave amplitude energy term in Hamiltonian (5). For high H, the spatial coupling terms become negligible, as their amplitude scales linearly with the wave's amplitude whereas the "kinetic" term scales quadratically. As a result, the system approaches a free wave limit.

The emergence of these chaotic regions in phase space was seen to be of a common type, namely, where chaos appears over and around separatrices, as illustrated by the series of portraits in Figs. 7 and 8, for H=0.5. Figure 7 shows portraits for varying  $\bar{P}$ , in a parameter range over the first quadrant  $(\bar{P}, \Delta_{\omega}>0)$  in Fig. 6, while Fig. 8 shows portraits for varying  $\Delta_{\omega}$  for values in the third quadrant  $(\bar{P}, \Delta_{\omega}<0)$ , as the system goes from regions with full regularity (A=1.0) through regions of co-existence with chaos (A<1.0). Normally, chaos occurs within limited regions of phase space and it coexists with invariant circles that are often seen for higher values of amplitude  $I_1$ .

In more detail, the chaotic layer as shown in Fig. 7 emerges around the main island centered at  $\phi_1=0$  (panel A) and increases as secondary bifurcations disrupt the island's invariant circles. Simultaneously, a pitchfork bifurcation further promotes chaos within the main island but from the inside out (panels B, C, and D). In panel C, it is seen that the chaotic domain, although fully connected, has a slower chaotic regime around the bifurcated pair of islands, with stickiness concentrated around this area. Finally, panels E and F show that the secondary resonant islands disappear, leaving a rather uniform chaotic sea (panel E) that further disappears, returning to

Chaos ARTICLE pubs.aip.org/aip/cha

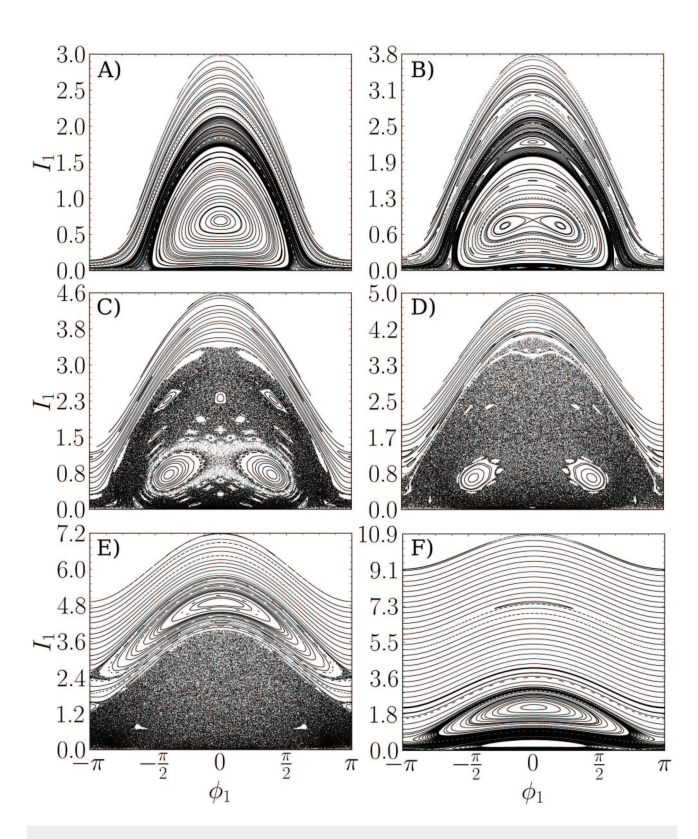


**FIG. 7.** Phase space portraits on the Poincaré section  $\Sigma$  [Eq. (11)]. (a)  $\bar{P}=0.5$ , (b)  $\bar{P}=1.0$ , (c)  $\bar{P}=1.5$ , (d)  $\bar{P}=1.75$ , (e)  $\bar{P}=3.0$ , (f)  $\bar{P}=5.0$ . In all cases, H=0.5 and  $\Delta_{\omega}=2.0$ .

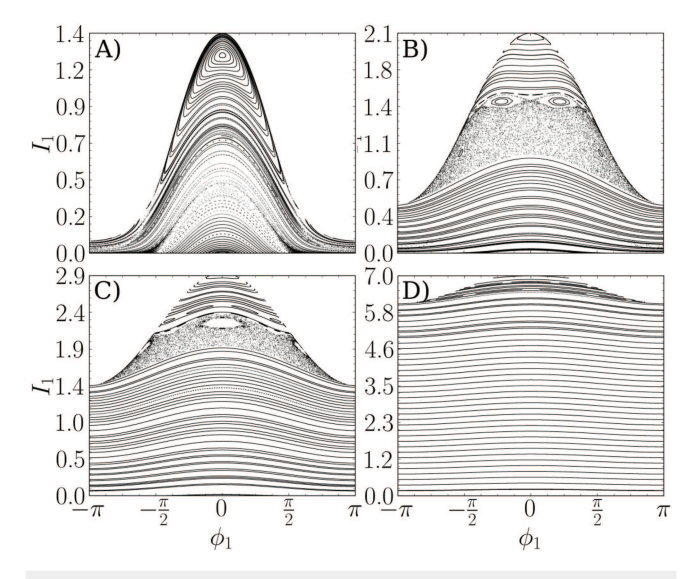


**FIG. 8.** Phase space portraits on the Poincaré section  $\Sigma$  [Eq. (11)]. (a)  $\Delta_{\omega}=-0.5$ , (b)  $\Delta_{\omega}=-4.0$ , (c)  $\Delta_{\omega}=-6.0$ , (d)  $\Delta_{\omega}=-15.0$ . In all cases, H=0.5 and  $\bar{P}=-1.0$ .

full regularity (panel F). In a slightly different manner, the transition shown in Fig. 8 corresponds to a chaotic layer emerging in between invariant regular sets (panels B and C), although with the same process of secondary bifurcations taking place.

#### V. CONCLUSIONS

In the simple scenario of one particle interacting with two waves, although, initially, a three degrees-of-freedom system, we show that simple canonical transformations yield a two degrees-of-freedom Hamiltonian with a clear connection to the original one. On top of the transformations, the only restrictive hypotheses made were the equal coupling parameter between each wave and the particle, and the equal wavenumber for both waves. The other assumptions made, i.e., the unit mass and unit coupling coefficients, can be made by rescaling variables without loss of generality. This simple form provides a framework to understand the mechanism of the emergence of chaos in the system as the particle acts as a mediator of energy-momentum exchange between the waves, which are assumed to be non-interacting in more basic models.

For this simplified Hamiltonian, it was shown that the number of equilibrium solutions has a non-trivial dependence on the control parameters, namely, the total momentum  $\bar{P}$  and frequency detuning  $\Delta_{\omega}=\omega_2-\omega_1$ . These equilibria correspond to any locked configuration, where the particle travels along with the waves while aligned with their extremum points. For any of these spatially locked states, the nonlinear nature of wave-particle coupling can yield up to four combinations of wave amplitudes allowing for equilibrium. Moreover, the highest number of equilibria combinations was found for  $\bar{P}>0$ , indicating that the waves require a minimum amount of momentum in order to carry the particle along with them. This comes as a consequence of the topology of the wave amplitude equilibrium function as two disjoint surfaces with concavity based on the type of locked position selected.

Despite the interaction between one particle and two waves being nearly integrable throughout most of the domain of its control parameters, the self-consistent coupling term added in our model was able to significantly induce chaos. In the limit where both the total momentum  $\bar{P}$  and the frequency detuning are small (up to an order of magnitude  $\bar{P} \approx 10$ ), the energy exchange between the waves, as mediated by the particle, is enough to destabilize trajectories. This possibility of energy-momentum exchange promoted by the non-linear coupling prevents the dynamics where the particle is either free or enslaved to one of the waves, as in the cases for large  $|\bar{P}|$ or  $|\Delta_{\omega}|$ . The emergence of chaos was seen around separatrices and higher order bifurcations, as usually observed in a KAM description. However, an ergodic limit, which could be related to the destabilization of the particle motion, was not found in the equal wave limit tested here, which could naturally be investigated as an extension of the current work.

Beyond the first exploratory results shown here, the extent to which the coupling strength parameters  $\beta_i$  can differ in order to promote enough energy-momentum exchange to produce chaos is still unclear. By assuming equal coupling strength, we restrict ourselves to cases where the dispersion relation is broad as a function of the wavelength, as in the case of a cold plasma. However,

30 May 2025 15:53:49

with different couplings, the imbalance between wave modes might suppress instabilities and, therefore, global chaos.

In the same way, a difference in wavenumbers could induce chaotic behavior, although the analysis in this case becomes cumbersome as the equations lose spatial periodicity and the number of free parameters increases. More generally, one could evaluate how to extend the energy-momentum exchange mechanism to the limit of many particles and waves, thus approaching the complete model.

#### **ACKNOWLEDGMENTS**

We acknowledge the financial support from the scientific agencies: São Paulo Research Foundation (FAPESP) under Grant No. 2018/03211-6; Conselho Nacional de Desenvolvimento Científico e Tecnológico (CNPq) under Grant Nos. 200898/2022-1 and 304616/2021-4; Coordenação de Aperfeiçoamento de Pessoal de Nível Superior (CAPES) and Comité Français d'Évaluation de la Coopération Universitaire et Scientifique avec le Brésil (COFECUB) under Grants CAPES/COFECUB 8881.143103/2017-1 and COFECUB 40273QA-Ph908/18. Centre de Calcul Intensif d'Aix-Marseille is also acknowledged for granting access to its high-performance computing resources. Y. Elskens is grateful to Serge Aubry for his fascinating lectures in 1985 at Beg-Rohu, which revealed more facets of Hamiltonian dynamics and its broader range of applications, and for the enthusiasm Serge always kindly shared with his audience.

#### **AUTHOR DECLARATIONS**

#### Conflict of Interest

The authors have no conflicts to disclose.

### **Author Contributions**

Matheus J. Lazarotto: Conceptualization (equal); Data curation (equal); Formal analysis (equal); Investigation (equal); Methodology (equal); Software (lead); Validation (equal); Visualization (equal); Writing – original draft (lead); Writing – review & editing (equal). Iberê L. Caldas: Conceptualization (equal); Data curation (equal); Formal analysis (equal); Funding acquisition (lead); Methodology (equal); Supervision (equal); Validation (equal); Visualization (equal); Writing – review & editing (equal); Formal analysis (equal); Funding acquisition (lead); Methodology (equal); Supervision (equal); Validation (equal); Visualization (equal); Writing – original draft (equal); Writing – review & editing (equal).

#### **DATA AVAILABILITY**

The data that support the findings of this study are available from the corresponding author upon reasonable request.

#### APPENDIX A: PARAMETER REDUCTION VIA SCALINGS

In the simplification step of Hamiltonian (2)–(4), we impose an equal wave number for both waves  $(k_1 = k_2 = k)$  as well as the coupling parameters with the particle  $(\beta_1 = \beta_2)$ , allowing one to set  $\epsilon \beta_1 = \epsilon \beta_2 = \beta$ . To eliminate k from within the coupling term, the position can be normalized to x' = kx. For the remaining

parameters, we set the global scaling factor

$$\alpha = (\beta^2/m)^{1/3} \tag{A1}$$

and rescale variables according to

$$\iota = \alpha \iota,$$

$$\omega_i' = \alpha^{-1} \omega_i, \tag{A2}$$

$$p'/p = I_1'/I_1 = I_2'/I_2 = P'/P = (m\beta)^{-2/3},$$

and

$$H' = (m\beta^4)^{-1/3}H.$$
 (A3)

The system in primed variables obtained from (2) is the reduced model (4) (for N = 1 and M = 2). This scaling also acts on the action so that  $S' = (m\beta)^{-2/3}S$ .

## APPENDIX B: CARTESIAN FORM OF THE EQUATIONS OF MOTION

Hamiltonian (6) yields the following equations of motion:

$$\dot{u}_{1} = \partial_{\nu_{1}} H' = \nu_{1} \left( \frac{1}{2} r - \bar{P} \right),$$

$$\dot{u}_{2} = \partial_{\nu_{2}} H' = \nu_{2} \left( \frac{1}{2} r - \bar{P} + \Delta_{\omega} \right),$$

$$\dot{v}_{1} = -\partial_{u_{1}} H' = -u_{1} \left( \frac{1}{2} r - \bar{P} \right) + 1,$$

$$\dot{\nu}_{2} = -\partial_{u_{2}} H' = -u_{2} \left( \frac{1}{2} r - \bar{P} + \Delta_{\omega} \right) + 1,$$
(B1)

where  $r := u_1^2 + v_1^2 + u_2^2 + v_2^2$ .

#### APPENDIX C: DEGENERATE LIMIT OF NULL DETUNING

In Hamiltonian (3) or (4), the case  $\omega_1 = \omega_2$  is degenerate [or equivalently for  $\Delta_{\omega} = 0$  in Hamiltonian (6) or (5)], as both waves have the same wavenumber and the same phase velocity. This is better investigated with the change of variables

$$\xi_1 = \frac{X_1 + X_2}{\sqrt{2}}, \quad \xi_2 = \frac{X_2 - X_1}{\sqrt{2}},$$

$$\eta_1 = \frac{Y_1 + Y_2}{\sqrt{2}}, \quad \text{and} \quad \eta_2 = \frac{Y_2 - Y_1}{\sqrt{2}},$$
(C1)

which is canonical. Then, the Hamiltonian can be expressed as follows:

$$H_{\text{sc}}^{1,2} = H_0(p, \eta_1, x, \xi_1) + H_2(\eta_2, \xi_2) + \frac{\Delta_\omega}{2} (\xi_1 \xi_2 + \eta_1 \eta_2),$$
 (C2)

with

$$H_0(p, \eta_1, x, \xi_1) = \frac{p^2}{2} + \bar{\omega} \left( \frac{\xi_1^2 + \eta_1^2}{2} \right) + \sqrt{2} \left( \eta_1 \sin(x) - \xi_1 \cos(x) \right),$$
(C3)

and

$$H_2(\eta_2, \xi_2) = \bar{\omega} \left( \frac{\xi_2^2 + \eta_2^2}{2} \right)$$
 (C4)

for  $\bar{\omega} := (\omega_1 + \omega_2)/2$ .

One recognizes in  $H_0$  the integrable model  $H^{1,1}_{\rm sc}$  (one wave, one particle) with frequency  $\bar{\omega}$  and coupling  $\sqrt{2}$ , and in  $H_2$ , a harmonic oscillator (with an eigenfrequency matching that of the wave in  $H_0$ ). When  $\Delta_{\omega}=0$ , these systems are uncoupled, and the limit  $\Delta_{\omega}\to 0$  can be investigated using KAM-type theory (noting that Hamiltonian  $H_2$  is degenerate as it has no shear).

In addition, a Galilean transformation can be used to set  $\bar{\omega}=0$ . Then, the limit  $\Delta_{\omega}\to 0$  can also lead to slow chaos. <sup>20–22</sup>

#### APPENDIX D: STABILITY OF LOCKED SOLUTIONS

By assuming the locked phases solution  $\phi_i^* = n_i \pi$  for  $n_i = 0, 1$  and i = 1, 2 and the corresponding amplitudes  $I_1^*, I_2^*$ , the Jacobian for equilibrium solutions reads

$$\mathbb{J} = \begin{pmatrix} 0 & 0 & f_1 & 1 \\ 0 & 0 & 1 & f_2 \\ g_1 & 0 & 0 & 0 \\ 0 & g_2 & 0 & 0 \end{pmatrix},$$

where  $f_i$  and  $g_i$  are defined as

$$f_i = f(I_i^*, n_i) := 1 + \frac{(-1)^{n_i}}{2\sqrt{2(I_i^*)^3}}$$

and

$$g_i = g(I_i^*, n_i) := -(-1)^{n_i} \sqrt{2I_i}$$
 for  $i = 1, 2$ .

Given the biquadratic form of the Jacobian's characteristic polynomial

$$\lambda^4 - (g_1 f_1 + g_2 f_2) \lambda^2 + g_1 g_2 (f_1 f_2 - 1) = 0,$$

one may solve it analytically for its eigenvalues  $\lambda_i$  as

$$\lambda_{\pm,\pm} = \pm \sqrt{\Lambda_{\pm}}$$
,

with

$$\Lambda_{\pm} = \frac{1}{2} \left( g_1 f_1 + g_2 f_2 \pm \sqrt{\left(g_1 f_1 - g_2 f_2\right)^2 + 4g_1 g_2} \right),$$

and where all the four possible sign combinations are considered in the notation  $\pm. \\$ 

#### APPENDIX E: DECOUPLING LIMIT

When analyzing the system with weak coupling, that is, in the limit  $\beta=m\ll 1$ , one recovers the paradigmatic 1.5-degree-of-freedom model of a particle slaved to two free waves. As done in Appendix A, we set  $k_1=k_2=k$  and  $\epsilon\beta_1=\epsilon\beta_2=\beta$  in Hamiltonian (2), for the case N=1, M=2. Setting p'=p/m in the equations of motion then yields

$$\ddot{x} = -\sqrt{2I_1}\sin(x - \theta_1) - \sqrt{2I_2}\sin(x - \theta_2),$$
$$\dot{I}_i = \beta\sqrt{2I_i}\sin(x - \theta_i),$$
$$\dot{\theta}_i - \omega_i = \beta(2I_i)^{-1/2}\cos(x - \theta_i),$$

so that the particle evolves with the waves whereas the waves themselves evolve under an  $O(\beta)$  feedback, becoming free waves in the

limit  $\beta \to 0$ . This scale separation does not satisfy the standard KAM hypotheses, as the wave dynamics are degenerate (harmonic oscillators).

An alternative way to apply KAM theory to the current model would be to consider Hamiltonian (5) in the form

$$H' = H_1(I'_1, \phi_1) + H_2(I'_2, \phi_2) + I'_1I'_2,$$

where

$$H_1 = I_1'^2 / 2 - \bar{P}I_1' - \sqrt{2I_1'} \cos \phi_1 \tag{E1}$$

and

$$H_2 = I_2'^2/2 - (\bar{P} - \Delta_\omega)I_2' - \sqrt{2I_2'}\cos\phi_2,$$
 (E2)

where both  $H_1$  and  $H_2$  reduce by a mere Galilean transformation to the N=M=1 integrable model, [Eq. (9) in Gomes *et al.*<sup>13</sup>]. We leave these analyses for future work.

#### **REFERENCES**

<sup>1</sup>Y. Elskens and D. Escande, *Microscopic Dynamics of Plasmas and Chaos* (IOP Publishing, Bristol, 2003).

<sup>2</sup>D. F. Escande and Y. Elskens, "Microscopic dynamics of plasmas and chaos: The wave-particle interaction paradigm," Plasma Phys. Control Fusion 45, A115–A124 (2003).

<sup>3</sup>R. Balescu, *Statistical Mechanics of Charged Particles* (Wiley-Interscience, London, 1963).

<sup>4</sup>F. Doveil, A. Macor, and K. Auhmani, "Wave-particle interaction investigated in a travelling wave tube," Plasma Phys. Control Fusion 47, A261–A271 (2005).

<sup>5</sup>M. C. de Sousa, F. Doveil, Y. Elskens, and I. L. Caldas, "Wave-particle interactions in a long traveling wave tube with upgraded helix," Phys. Plasmas 27(9), 093108 (2020).

<sup>6</sup>A. Macor, F. Doveil, and Y. Elskens, "Electron climbing a "devil's staircase" in wave-particle interaction," Phys. Rev. Lett. **95**, 264102 (2006).

<sup>7</sup>E. Ott, Chaos in Dynamical Systems (Cambridge University Press, New York, 1993).

<sup>8</sup>G. R. Smith and N. R. Pereira, "Phase-locked particle motion in a large-amplitude

plasma wave," Phys. Fluids 21, 2253–2262 (1978).

9 N. Besse, Y. Elskens, D. F. Escande, and P. Bertrand, "Validity of quasilinear theory: Refutations and new numerical confirmation," Plasma Phys. Control. Fusion 53(025012), 36 (2010).

<sup>10</sup>T. M. O'Neil, J. H. Winfrey, and J. H. Malmberg, "Nonlinear interaction of a small cold beam and a plasma," Phys. Fluids 14(6), 1204–1212 (1971).

<sup>11</sup>I. N. Onishchenko, A. R. Linetskii, N. G. Matsiborko, V. D. Shapiro, and V. I. Shevchenko, "Contribution to the nonlinear theory of excitation of a monochromatic plasma wave by an electron beam," JETP Lett. **12**(8), 281–285 (1970).

<sup>12</sup>H. E. Mynick and A. K. Kaufman, "Soluble theory of nonlinear beam-plasma interaction," Phys. Fluids 21, 653–663 (1978).

<sup>13</sup>J. V. Gomes, M. C. de Sousa, R. L. Viana, I. L. Caldas, and Y. Elskens, "Low-dimensional chaos in the single wave model for self-consistent wave-particle Hamiltonian," Chaos 31, 083104 (2021).

<sup>14</sup>J. C. Adam, G. Laval, and I. Mendonça, "Time-dependent nonlinear Langmuir waves," Phys. Fluids 24, 260–267 (1981).

<sup>15</sup>D. del Castillo-Negrete, "Dynamics and self-consistent chaos in a mean field Hamiltonian model," in *Dynamics and Thermodynamics of Systems with Long-Range Interactions*, edited by T. Dauxois, S. Ruffo, E. Arimondo, and M. Wilkens (Springer, Berlin, 2002), pp. 407–436.

<sup>16</sup>B. V. Chirikov, "A universal instability of many-dimensional oscillator systems," Phys. Rep. 52(5), 263–379 (1979).

<sup>17</sup>D. F. Escande, "Stochasticity in classical Hamiltonian systems: Universal aspects," Phys. Rep. 121(3–4), 165–261 (1985).

<sup>18</sup>C. Skokos, T. Bountis, C. G. Antonopoulos, and M. N. Vrahatis, "Detecting order and chaos in Hamiltonian systems by the SALI method," J. Phys. A: Math. Gen. 37, 6269–6284 (2004).

Chaos ARTICLE pubs.aip.org/aip/cha

<sup>&</sup>lt;sup>19</sup>G. A. Gottwald, C. H. Skokos, and J. Laskar, Chaos Detection and Predictability

<sup>(</sup>Springer-Verlag, Berlin, 2015). <sup>20</sup>Y. Elskens and D. F. Escande, "Slowly pulsating separatrices sweep homoclinic tangles where islands must be small—An extension of classical adiabatic theory," Nonlinearity 4, 615–667 (1991).

<sup>&</sup>lt;sup>21</sup> A. I. Neishtadt, V. V. Sidorenko, and D. V. Treschev, "Stable periodic motions in the problem on passage through a separatrix," Chaos 7(2), 1–11 (1997).

22 A. I. Neishtadt, C. Simó, D. Treschev, and A. Vasiliev, "Periodic orbits and stability islands in chaotic seas created by separatrix crossings in slow-fast systems," Discrete Contin. Dyn. Syst. Ser. B **10**(2/3), 621–650 (2008).